Journal of Power Sources 248 (2014) 874–885

Contents lists available at ScienceDirect

Journal of Power Sources

journal homepage: www.elsevier.com/locate/jpowsour

Effects of oxidation on structure and performance of $LiVPO_4F$ as cathode material for lithium-ion batteries

Rui Ma, Lianyi Shao, Kaiqiang Wu, Miao Shui, Dongjie Wang, Nengbing Long, Yuanlong Ren, Jie Shu*

Faculty of Materials Science and Chemical Engineering, Ningbo University, Ningbo 315211, Zhejiang Province, People's Republic of China

HIGHLIGHTS

- $LiVPO_4F$ transforms into $Li_{1-x}VPO_4F_{1-y}O_z$ after oxidization in air.
- A transformation of $LiVPO_4F \rightarrow Li_{0.72}VPO_4F \rightarrow VPO_4F$ appears for $LiVPO_4F$ during charge.
- $Li_{1-x}VPO_4F_{1-y}O_z$ shows stable structure upon delithiation.

GRAPHICAL ABSTRACT

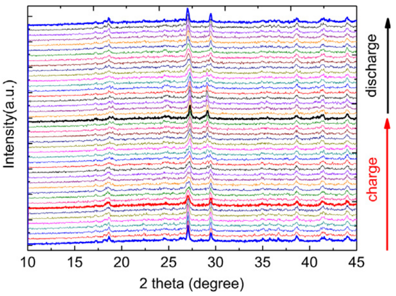

ARTICLE INFO

Article history:
Received 13 August 2013
Received in revised form
21 September 2013
Accepted 9 October 2013
Available online 17 October 2013

Keywords:
Fluorophosphate
Oxidation
Cathode material
Lithium-ion batteries
In-situ X-ray diffraction

ABSTRACT

In this paper, a series of $LiVPO_4F$-based samples are prepared through sintering $LiVPO_4F$ at different temperatures under air. Experimental results show that the pristine sample is oxidized to a new compound $Li_{1-x}VPO_4F_{1-y}O_z$ ($0 < x < 0.2$, $0.9 < y \leq 1$, $0.9 < z \leq 1$) with similar structure of $LiVPO_4O$ under air at 550 °C or higher one. *In-situ* X-ray diffraction patterns indicate that the original material $LiVPO_4F$ undergoes two two-phase structural evolutions upon Li^+ electrochemical extraction at average operating potentials at 4.26 and 4.30 V, corresponding to the continuous transformation of $LiVPO_4F \rightarrow Li_{0.72}VPO_4F \rightarrow VPO_4F$ in the first charge process. In the reverse discharge process, there is only one two-phase structural transition $VPO_4F \rightarrow LiVPO_4F$ without the appearance of the intermediate phase $Li_{0.72}VPO_4F$ on Li^+ insertion reaction at 4.18 V. Therefore, the extraction/insertion process of $LiVPO_4F$ is an asymmetrical phase transformation. When the sintering temperature is raised to 550 °C, $Li_{1-x}VPO_4F_{1-y}O_z$ exhibits extremely poor electrochemical performance, which is attributed to the volatilization loss of lithium and the replacement of fluorine by oxygen in the structure during the sintering process under air. However, $Li_{1-x}VPO_4F_{1-y}O_z$ has a very stable structure during the whole process of galvanostatic charge/discharge cycles as confirmed by *in-situ* X-ray diffraction technique.

1. Introduction

In the past ten years, lithium-ion batteries have been extensively applied to various portable electronic products, such as laptops, cell phones and digital cameras, resulted from miniaturization technologies. Nowadays, the application of lithium-ion batteries in large-scale devices such as power electric and hybrid electric vehicles, energy-efficient cargo ship, locomotives and aerospace are being driven by an ever-increasing demand, seriously environmental issues and ever-increasing cost of fossil fuels. However, there are many key factors in electrode materials, such as working potential, energy density, power capability, cycle lifetime, stable

---

* Corresponding author. Tel.: +86 574 87600787; fax: +86 574 87609987.
E-mail addresses: sergio_shu@hotmail.com, shujie@nbu.edu.cn (J. Shu).

0378-7753/$ – see front matter © 2013 Elsevier B.V. All rights reserved.
http://dx.doi.org/10.1016/j.jpowsour.2013.10.029

structure and security problems, need to be improved before lithium-ion batteries could be applied to large-scale devices [1–6]. Owing to the pivotal role of cathode materials in high power lithium-ion batteries, much attention is paid to the development of cathode materials such as layer-structured $LiMO_2$ (M = Co, Ni, Mn) [7,8], spinel-structured $LiMn_2O_4$ [9,10], olivine-structured $LiMPO_4$ (M = Fe, Mn, Co) [11–15], vanadium oxide (V_2O_5, LiV_3O_8) [16–18], Nasicon-type $Li_xM_2(PO_4)_3$ (M = Fe, V, Ti) [19], fluorine-containing transition metal phosphates and sulfates $A_xM(XO_4)F$ (A = Li; M = V, Fe, Ti; X = P, S) [20–24].

Inspired pioneering work by Barker [25,26], $LiVPO_4F$, as an attractive cathode material for the next generation of lithium-ion batteries, is a novel fluorophosphate material based on the phosphate polyanion. In the crystal structure, the strong inductive effect of the PO_4^{3-} polyanion moderates the energetics of the transition-metal redox couple to generate the relatively high operating potentials. Additionally, the effect of the presence of additional fluorine atom on this inductive effect in the structure of $LiVPO_4F$ is beneficial to develop novel polyanion systems in the future, i.e. the V–F bond is very stable, which results in the structure of $LiVPO_4F$ remaining stable upon repeated Li^+ extraction/insertion reactions [26]. However, $LiVPO_4F$ exposed to air/moisture is difficult to avoid the surface oxidation and moisture-absorption, which will result in the structural changes of $LiVPO_4F$. As a result, it may show poor electrochemical performance due to partial vanadium oxidation and/or lithium and fluorine loss similar with those appeared on oxidized $LiFePO_4$ [27].

Therefore, this work is to investigate the effects of oxidation on the structure and performance of $LiVPO_4F$ as cathode materials for lithium-ion batteries through a combination of several powerful techniques such as thermogravimetry and differential thermal analysis (TG–DTA), thermogravimetry, differential scanning calorimetry and mass spectrometry (TG–DSC–MS), inductively coupled plasma atomic emission spectrometer (ICP-AES), energy dispersive spectrometer (EDS), X-ray fluorescence spectrometer (XRF), X-ray photoelectron spectrometer (XPS), Fourier transform infrared spectrometer (FTIR), powder and *in-situ* X-ray diffraction (XRD) techniques. It is found that the pristine $LiVPO_4F$ shows an asymmetrical structural evolution but oxidized $LiVPO_4F$ with similar structure of $LiVPO_4O$ shows almost no structural transformation during charge/discharge process.

2. Experimental

2.1. Synthesis of $LiVPO_4F$-based samples

The synthesis of pristine $LiVPO_4F$ was similar with the method reported by Barker [9]. Firstly, V_2O_5 (AR, ≥99.0%), $NH_4H_2PO_4$ (AR, ≥99.0%) and acetylene black (25% mass excess) with a stoichiometric amount were mixed and sintered to yield the intermediate phase VPO_4, and then LiF was added to obtain the original material $LiVPO_4F$. Detailed synthetic steps of $LiVPO_4F$ were reported in our previous paper [28]. Afterward, a series of $LiVPO_4F$-based samples were prepared through sintering $LiVPO_4F$ over a temperature range between 350 and 750 °C for 30 min under air.

2.2. Electrode and cell preparation

The working electrode was prepared by mixing 80% $LiVPO_4F$-based samples and 10% polyvinylidene fluoride and 10% carbon black. This powder mixture was manually ground and then dissolved in N-methylpyrodine to form homogeneous slurry, and then the slurry was coated on Al foil, dried at 120 °C for 12 h in a vacuum oven, and cut into discs with a diameter of 15 mm. For cell fabrication, the counter electrode is Li metal disc, the separator is Whatman glass fiber diaphragm, and the electrolyte is comprised of 1 mol L^{-1} $LiPF_6$ in ethylene carbonate and dimethyl carbonate with a volume ratio of 1:1.

2.3. Analytical methods

The thermogravimetry and differential thermal analysis behaviors of $LiVPO_4F$ were investigated on a Seiko TG/DTA 6300 instrument under air over a temperature range between 20 and 800 °C with a heating rate of 5 °C min^{-1}. The cooling process was conducted under natural conditions. Thermogravimetry, differential scanning calorimetry and mass spectrometry tests were performed by a NETSCH STA 449C combined with a NETSCH 403C Aeolos II quadrupole mass spectrometer. The test temperature range was from 30 to 550 °C with a heating rate of 10 °C min^{-1} under argon with an oxygen flowing rate of 18 ml min^{-1}. Simultaneously, the gaseous products formed in thermal reaction were monitored by the connected mass spectrometer. Powder X-ray diffraction patterns were collected on a Bruker D8 Focus diffractometer (40 kV, 40 mA), using Cu-Kα radiation. The scanning angle 2θ was in a range from 10 to 80° with a scanning rate of 4° min^{-1}. The surface morphologies and element compositions of $LiVPO_4F$-based samples were characterized by Hitachi S3400 scanning electron microscopy (SEM) and Oxford INCA energy dispersive spectrometer. Inductively coupled plasma atomic emission spectrometer (Perkin Elmer Optima 2100 DV) was employed to determine the mole ratio (At.%) of Li, P and V in the original $LiVPO_4F$ and the oxidized samples. The valence states of vanadium in the original $LiVPO_4F$ and the samples sintered at 550 °C for 30 min under air were determined by X-ray photoelectron spectrometer (Kratos Model XSAM800) equipped with an Mg Kα achromatic X-ray source ($h\nu$ = 1235.6 eV). X-ray fluorescence spectrometer (Bruker S2 Ranger) was employed to determine the mole ratio (At.%) of P and V in the original $LiVPO_4F$ and the samples sintered at 550 °C for 30 min under air. Fourier transform infrared spectroscopy measurements were carried out on Shimadzu FTIR-8900 spectrometer with a distinguishability of 4 cm^{-1} between 400 and 4000 cm^{-1} $LiVPO_4F$-based samples were manually ground with KBr and then pressed into thin slices for FTIR analysis.

The galvanostatic charge/discharge tests were performed on LAND CT2001A battery test system (Wuhan Jinnuo, China). Lithium-ion batteries were cycled between 3.0 and 4.7 V at a current density of 10 mA g^{-1}. Cyclic voltammetry (CV) tests were performed between 3.0 and 4.7 V with a scanning rate of 0.1 mV s^{-1} on CHI 660D electrochemical workstation (Shanghai Chenhua, China) at room temperature.

The *in-situ* structural evolutions of $LiVPO_4F$ and the oxidized sample obtained at 550 °C during Li^+ extraction/insertion were observed by *in-situ* X-ray diffraction using the same Bruker D8 Focus diffractometer as described above. Prior to the *in-situ* X-ray diffraction tests, $LiVPO_4F$ powders and the oxidized sample were respectively mixed with carbon black and subsequently ground in agate mortar and then ready for the following *in-situ* X-ray diffraction tests. All simulated cells and *in-situ* cells were assembled in an argon-filled glovebox with relative humidity under 5 ppm.

The homemade *in-situ* cell used in this work is designed based on the adjustment of *in-situ* Raman cell reported by our previous paper [29,30]. It mainly consists of stainless steel chamber, beryllium disc, working electrode, separator, lithium disc, stainless steel disc and polytetrafluoroethylene sleeve. Dozens of milligrams powders mixed with carbon black were prepared in advance as the working electrode by directly putting on the beryllium window of the *in-situ* cell, and then separator, lithium metal, stainless steel disc and electrolyte are placed in turn in the *in-situ* cell chamber. All the collected *in-situ* X-ray diffraction data were analyzed using the Fullprof program.